Fixed Switching Frequency Model Predictive Control for Parallel Inverters in Microgrids

Fernanda Carnielutti[1], **Mokhtar Aly**[2], **Margarita Norambuena**[3], **Jiefeng Hu**[4],
Josep Guerrero[5,6], **Jose Rodriguez**[2]

[1]Federal University of Santa Maria, Department of Electrical Energy Processing, Santa Maria, RS Brazil.
[2]Universidad San Sebastian, Santiago, Chile.
[3]Universidad Tecnica Federico Santa Maria, Valparaíso, Chile.
[4]Federation University, Ballarat, Australia.
[5]Aalborg University, Aalborg, Denmark.
[6]Technical University of Catalonia, Barcelona, Spain.

e-mail: fernanda.carnielutti@ufsm.br, mokhtar.aly@uss.cl, margarita.norambuena@usm.cl, j.hu@federation.edu.au,
josep.m.guerrero@upc.edu, jose.rodriguezp@uss.cl

ABSTRACT A Fixed-Switching-Frequency Model Predictive Control (FSF-MPC) for Master-Slave inverters in microgrids is proposed in this paper. The Master is a three-phase, two-level inverter with an LC filter, while the Slave is a three-phase, two-level inverter with an LCL filter. The inverters are connected in parallel in a microgrid, composed of different loads. The voltage and current inner control loops of the Master-Slave FSF-MPC are presented for both inverters. Then, two modes of operation are proposed: grid-connected and islanded, and the primary control for both cases is developed. Finally, Hardware-in-the-Loop (HIL) results are presented for different operational conditions of the microgrid with load-related disturbances. The HIL results validate the good performance of the proposed Master-Slave FSF-MPC, including fast dynamic response, multi-objective control, and fixed switching frequency.

KEYWORDS Master-Slave, Microgrids Model Predictive Control, Parallel Inverters

I. INTRODUCTION

Microgrids are systems comprised of distributed generation units with power electronics converters, lines, loads, relays, and communication systems. Hierarchical control is often used for microgrids, implemented as multi-loop cascaded linear controllers and modulators, such as centralized or distributed control, average load sharing, Master-Slave, and Droop [1], [2]. Specifically regarding Master-Slave, in [3], a robust controller was proposed using nested linear quadratic regulators and mixed H_2/H_∞ optimal control. A linear controller with cooperative load sharing was presented in [4] for multiple Master-Slave microgrids. A decentralized control was presented in [5]. Master-Slave strategies with Neural Networks were proposed in [6], [7]. Although these approaches are widely used, they present some disadvantages, such as inherent slow dynamic responses, difficulties to implement multi-objective control [1], and complex tuning procedures and/or large amounts of data for tuning.

An alternative for linear controllers for microgrids is the Finite-Control-Set MPC (FCS-MPC), where the discrete-time model of the system and its inputs are used to predict its future states [1], [2], [8], [9]. A cost function is defined and calculated for all system inputs at each sampling instant k. The input with the minimum value of its cost function is selected and implemented by the inverter during the switching period T_s. The cost function is designed to include multiple control objectives and non-linearities, accounting for system constraints and achieving faster dynamic responses compared to linear controllers [2]. As a result, FCS-MPCs can be used for microgrid applications, covering primary [10]–[12], secondary [13] and tertiary control [14], [15].

However, FCS-MPC presents some disadvantages, such as widespread harmonics and variable switching frequency. To overcome this, MPCs with fixed switching frequency (FSF-MPC) were proposed. In [16], a FSF-MPC for a five-level active neutral-point clamped (5L-ANPC) converter was presented, which reduces the computational burden when compared to FCS-MPC. The Space Vector Modulated MPC (SVM²PC) was presented in [17], combining control and modulation in a convex optimization problem with fast dynamic response and low computational burden. In [18], a Modulated MPC (MMPC) was presented. The duty cycles of the voltage vectors are calculated with the MMPC and applied to a PWM modulator, resulting in constant switching frequency. A modified version based on optimized over-modulation was presented in [19]. A two-vector Model-Free MPC was introduced in [20] for two-level three-phase inverters. A sequential MMPC was presented for single-phase grid-tied PV systems [21], [22], where the sequential evaluation of different control objectives eliminates the weighting factors. Even though various papers proposed FSF-MPCs, they have not been extensively used in microgrids.

In this context, this paper proposes an FSF-MPC for Master-Slave inverters in microgrids that is an extension
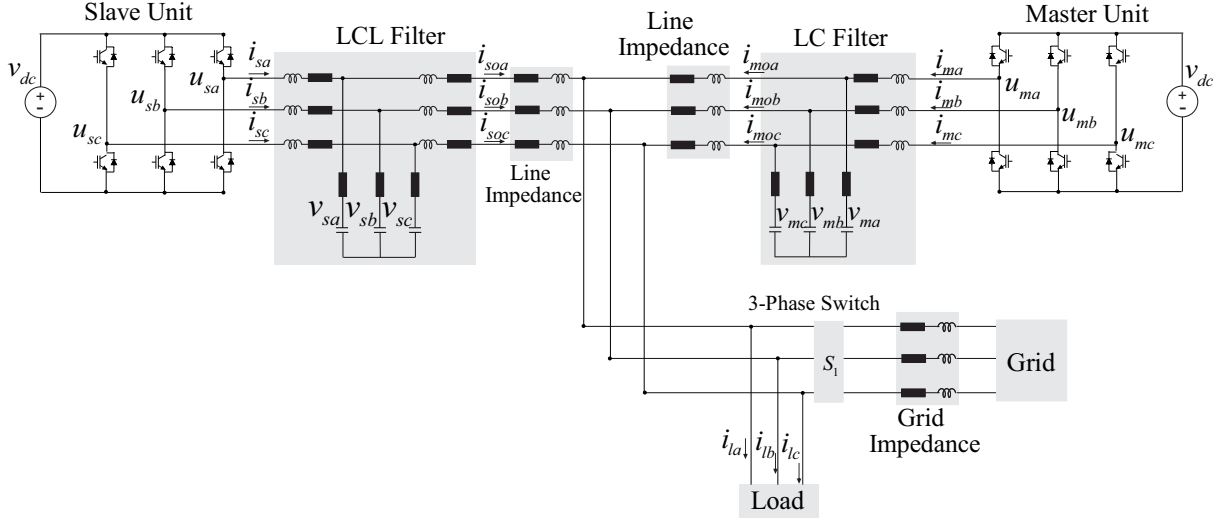
FIGURE 1. Microgrid considered as an example for the proposed Master-Slave FSF-MPC.

of [23]. In this work, the Master is a two-level three-phase inverter with LC filter, while the Slave is a two-level three-phase inverter with LCL filter. Two different operational modes are proposed for the microgrid: grid-connected and islanded. In grid-connected mode, both the Master and Slave are grid-following inverters. During islanded operation, the Master operates as a grid-forming inverter, while the Slave remains a grid-following inverter. The primary control for both cases is presented. The microgrid considered as an example has linear and nonlinear loads, and the grid and line impedances were included in the system. Advantages of the proposed FSF-MPC include fast dynamic response, multi-objective control, power sharing, and fixed switching frequency. As a result, it is able to bring together the main advantages of FCS-MPC and linear control. Finally, Hardware-in-the-Loop (HIL) results are presented for different operational conditions of the microgrid. The main contributions of the proposed Master-Slave FSF-MPC are:

- It presents the main advantages of both FCS-MPC (fast dynamic response and multi-objective control) and linear modulators (fixed switching frequency);
- It can operate grid-connected and islanded;
- It presents good performance under different load variations and unmodeled dynamics while performing power sharing among the inverters in the microgrid.

The main improvements with respect to [23] are:

- An extended literature review is included;
- A more detailed description of the FSF-MPC for the Master and Slave inverters is presented;
- The description of the primary control of the Master is included for grid-connected and islanded modes;
- More HIL results are shown, including the analysis of the operation of the proposed FSF-MPC and its comparison to a FCS-MPC.

II. MASTER-SLAVE FIXED SWITCHING FREQUENCY MPC
The system used as an example is presented in Fig.1, and the control block diagram is shown in Fig.2. The microgrid of Fig.1 is composed of two three-phase two-level inverters, one with LC filter and the other with LCL filter (the Master and Slave, respectively), a load, grid, and line impedance and a three-phase switch to connect and disconnect the microgrid to the main grid. Also, damping resistors are included in series with the filter capacitors of both inverters.

A. Master Inverter
The main objective of the Master is to control the filter capacitor voltages. The discrete-time models of the inverter-side currents and capacitor voltages in $\alpha\beta$ coordinates are (using the amplitude invariant Clark transformation):

$$
\begin{bmatrix} i_{m\alpha}(k+1) \\ i_{m\beta}(k+1) \end{bmatrix} = (1 - \frac{RT_s}{L_m}) \begin{bmatrix} 1 & 0 \\ 0 & 1 \end{bmatrix} \begin{bmatrix} i_{m\alpha}(k) \\ i_{m\beta}(k) \end{bmatrix} +
$$
$$
\frac{T_s}{L_m} \begin{bmatrix} 1 & 0 \\ 0 & 1 \end{bmatrix} \begin{bmatrix} u_{m\alpha}(k) \\ u_{m\beta}(k) \end{bmatrix} - \frac{T_s}{L_m} \begin{bmatrix} 1 & 0 \\ 0 & 1 \end{bmatrix} \begin{bmatrix} v_{m\alpha}(k) \\ v_{m\beta}(k) \end{bmatrix} \quad (1)
$$

$$
\begin{bmatrix} v_{m\alpha}(k+2) \\ v_{m\beta}(k+2) \end{bmatrix} = \begin{bmatrix} v_{m\alpha}(k+1) \\ v_{m\beta}(k+1) \end{bmatrix} +
$$
$$
\frac{T_s}{C_m} \begin{bmatrix} 1 & 0 \\ 0 & 1 \end{bmatrix} \begin{bmatrix} i_{m\alpha}(k+1) \\ i_{m\beta}(k+1) \end{bmatrix} - \frac{T_s}{C_m} \begin{bmatrix} 1 & 0 \\ 0 & 1 \end{bmatrix} \begin{bmatrix} i_{mo\alpha}(k+1) \\ i_{mo\beta}(k+1) \end{bmatrix}
$$
$$
(2)
$$

where $i_{m\alpha\beta}$ and $i_{mo\alpha\beta}$ are, respectively, the inverter-side and output currents, $u_{m\alpha\beta}$ are the inverter voltages, $v_{m\alpha\beta}$ are the filter capacitor voltages, T_s is the sampling period and L_m, C_m and R are the filter components. Two modes are proposed for the primary control of the Master: grid-connected and islanded, with different control objectives.
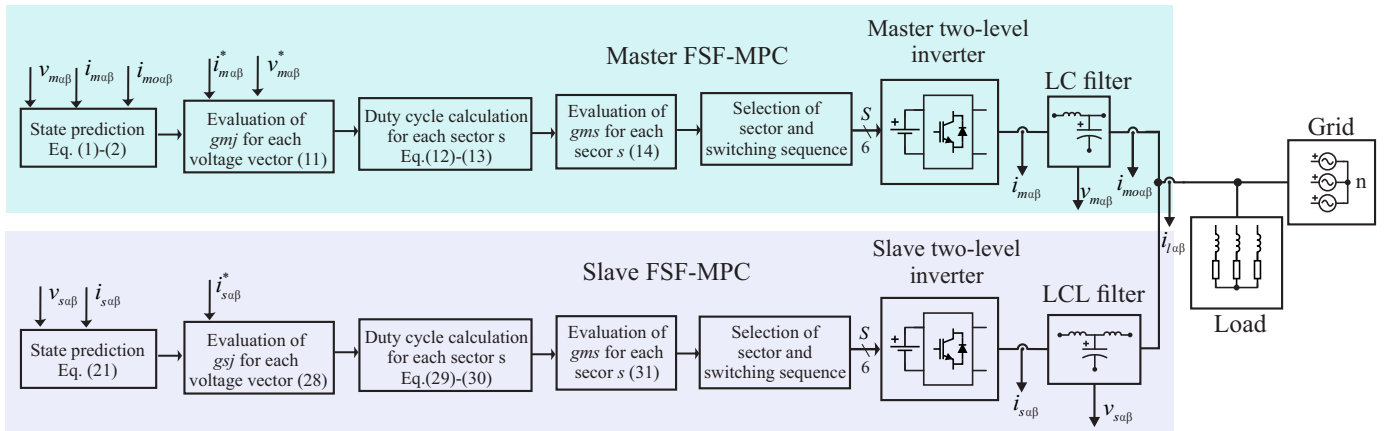
FIGURE 2. Block diagram for the proposed Master-Slave FSF-MPC.

1) Primary Control for Grid-Connected Operation

In this mode, the microgrid is connected to the grid, and the voltages are imposed by the grid. The Master is controlled as a grid-following inverter with a Synchronous-Reference-Frame Phase-Locked-Loop (SRF-PLL) [24]. The Master controls the voltages of the filter capacitors and the inverter-side currents, allowing the control of the active and reactive powers injected into the grid. The instantaneous power theory is used, together with an open-loop PQ control [24]. As a result, the current references for the Master are:

$$i_{mo\alpha}^*(k) = \frac{2}{3} \frac{v_{m\alpha}(k)P_m^*(k) + v_{m\beta}(k)Q_m^*(k)}{v_{m\alpha}^2(k) + v_{m\beta}^2(k)} \quad (3)$$

$$i_{mo\beta}^*(k) = \frac{2}{3} \frac{v_{m\beta}(k)P_m^*(k) - v_{m\alpha}(k)Q_m^*(k)}{v_{m\alpha}^2(k) + v_{m\beta}^2(k)} \quad (4)$$

where P_m^* and Q_m^* are the active and reactive power references, that can come from a microgrid central controller (MGCC). However, these are the references for the grid-side currents, and the inverter-side currents are controlled. In order to obtain the inverter-side current references, the reactive power of the LC filter is compensated as:

$$i_{m\alpha}^*(k) = i_{mo\alpha}^*(k) - 2\pi f C_m v_{m\beta}(k) \quad (5)$$

$$i_{m\beta}^*(k) = i_{mo\beta}^*(k) + 2\pi f C_m v_{m\alpha}(k) \quad (6)$$

where f is the grid frequency that comes from the SRF-PLL. Then, the references are extrapolated to $(k+1)$:

$$i_{m\alpha}^*(k+1) = i_{m\alpha}^*(k)cos(\omega T_s) - i_{m\beta}^*(k)sin(\omega T_s) \quad (7)$$

$$i_{m\beta}^*(k+1) = i_{m\beta}^*(k)cos(\omega T_s) + i_{m\alpha}^*(k)sin(\omega T_s) \quad (8)$$

The voltage references for the Master can be defined as the voltages measured at the Point of Common Coupling (PCC), considered here as the point after the LC filter where the inverter is connected to the grid. They are extrapolated to $(k+2)$ using the same procedure of (7)-(8):

$$v_{m\alpha}^*(k+2) = v_{PCC\alpha}^*(k)cos(2\omega T_s) - v_{PCC\beta}^*(k)sin(2\omega T_s) \quad (9)$$

$$v_{m\beta}^*(k+2) = v_{PCC\beta}^*(k)cos(2\omega T_s) + v_{PCC\alpha}^*(k)sin(2\omega T_s) \quad (10)$$

The cost function includes voltage and current control:

$$g_{mj} = \lambda_1(\mathbf{v}_{m\alpha\beta}^*(k+2) - \mathbf{v}_{mj\alpha\beta}(k+2))^2 + \\ \lambda_2(\mathbf{i}_{m\alpha\beta}^*(k+1) - \mathbf{i}_{mj\alpha\beta}(k+1))^2 + lim \quad (11)$$

where λ_1 and λ_2 are weighting factors, $\mathbf{v}_{m\alpha\beta}^*(k+2)$ and $\mathbf{i}_{m\alpha\beta}^*(k+1)$ are vectors with the voltage and current references, $j = 0...7$ are the inverter voltage vectors and $\mathbf{v}_{mj\alpha\beta}(k+2))^2$ and $\mathbf{i}_{mj\alpha\beta}(k+1))^2$ are, respectively, the predicted capacitor voltages and inverter-side currents for voltage vector j. The term lim limits the inverter-side currents to protect the semiconductor devices. If the norm of $\mathbf{i}_{mj\alpha\beta}$ is greater than the inverter maximum current, lim assumes a large value, and zero otherwise [25], [26].

For each T_s, $\mathbf{v}_{mj\alpha\beta}(k+2))$ and $\mathbf{i}_{mj\alpha\beta}(k+1))$ are predicted for all 8 inverter voltage vectors with (1)-(2) and cost function (11) is calculated. A switching sequence is defined offline for half the carrier period for each sector of the inverter SV diagram (shown in Fig. 3), using two non-null vectors and both redundancies of the null vector. A triangular carrier is used, with sampling at the underflow and period match. During the first half of T_s, the sequence of Table 1 is implemented and, during the second half, the mirrored sequence. The next step is the selection of the sector and its switching sequence to be implemented. The duty cycles for the three vectors in each sector are [16]:

$$d_a = \frac{g_{mb}g_{mc}}{G} \quad d_b = \frac{g_{ma}g_{mc}}{G} \quad d_c = \frac{g_{ma}g_{mb}}{G} \quad (12)$$

$$G = (g_{mb}g_{mc} + g_{ma}g_{mc} + g_{ma}g_{mb}) \quad (13)$$

where $d_a + d_b + d_c = 1$. The cost function of each sector is:

$$g_{ms} = d_a g_{ma} + d_b g_{mb} + d_c g_{mc} \quad (14)$$

where $s = 1...6$ are the sectors and a, b, c are the three vectors in each sector, organized in the switching sequence of Table 1. Finally, the sector with the lowest value of cost function g_{ms} is selected, and its switching sequence is implemented. This is depicted in the upper part of Fig.2.
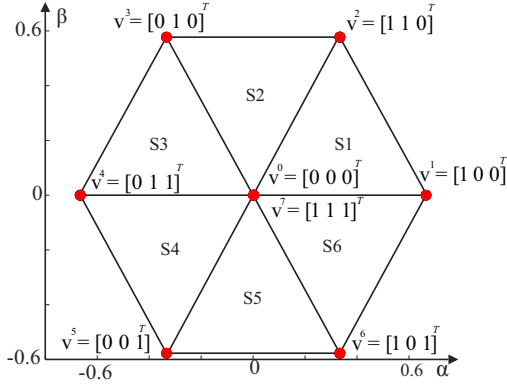
FIGURE 3. Normalized SV diagram of a three-phase two-level inverter.

TABLE 1. Switching sequences for each sector of the SV diagram.

Sector	Switching Sequence			
	a	b	c	a
S1	v^0	v^1	v^2	v^7
S2	v^0	v^3	v^2	v^7
S3	v^0	v^3	v^4	v^7
S4	v^0	v^5	v^4	v^7
S5	v^0	v^5	v^6	v^7
S6	v^0	v^1	v^6	v^7

TABLE 2. System parameters for the case studies.

Parameter	Value
DC-link voltage	800V
Rated power (Master and Slave)	100kVA
Maximum peak current (Master and Slave)	250A
LCL filter (Slave)	500μH; 100μF; 50μH
LC filter (Master)	500μH; 300μF
R (Master and Slave)	1.2Ω
Damping resistor (Master)	0.1Ω
Damping resistor (Slave)	1.0Ω
Grid impedance	$Z_g = 2.7\mu$H, 0.01Ω
Line impedance	$Z_l = 20\mu$H, 0.01Ω
Grid voltage (line-to-neutral)	220Vrms; 50Hz
Sampling and switching frequencies f_s and f_c	20kHz and 10kHz

2) Primary Control for Islanded Operation

The Master operates as a grid-forming inverter, generating the microgrid voltages. It also provides half the load power, performing power-sharing with the Slave. To do so, an outer Droop control is implemented. When the inner loops of the grid-forming inverter are implemented with MPC, a faster transient response is obtained when compared to linear controllers [25], [26]. Considering a resistive virtual impedance, the Droop law is:

$$v^*(k) = v_{nom} - k_p(P_m^* - P_m(k)) \qquad (15)$$

$$\omega^*(k) = \omega_{nom} + k_q(Q_m^* - Q_m(k)) \qquad (16)$$

where v^* is the amplitude voltage reference, v_{nom} is the desired microgrid voltage, ω^* is the reference frequency,

ω_{nom} is the desired microgrid frequency, k_p and k_q are the Droop coefficients, and P_m and Q_m are the instantaneous active and reactive powers of the Master, calculated as:

$$P_m(k) = v_{m\alpha}(k)i_{mo\alpha}(k) + v_{m\beta}(k)i_{mo\beta}(k) \qquad (17)$$

$$Q_m(k) = v_{m\beta}(k)i_{mo\alpha}(k) - v_{m\alpha}(k)i_{mo\beta}(k) \qquad (18)$$

No filters are used to calculate P_m and Q_m [25], [26]. The voltage references for the Master are defined as:

$$v_{m\alpha}^*(k) = v^*(k)cos(\omega T_s) - R_v i_{mo\alpha}(k) \qquad (19)$$

$$v_{m\beta}^*(k) = v^*(k)sin(\omega T_s) - R_v i_{mo\beta}(k) \qquad (20)$$

where R_v is the virtual resistance. The voltage references are extrapolated to $(k+2)$ as in (9)-(10). The procedure to obtain the current references is the same as in (3)-(8), but now the active and reactive power references are half the active and reactive load powers. The cost function is the same as in (11), and the FSF-MPC is implemented as in (12)-(14).

B. Slave Inverter

For the Slave inverter, the FSF-MPC procedure is the same as for the Master. However, the Slave operates as a grid-following inverter in both modes. A SRF-PLL is used to synchronize the Slave to the grid in grid-connected mode and to the Master when islanded. Its main objective is to control the currents injected into the load/grid. The inverter-side currents in $\alpha\beta$ coordinates are:

$$\begin{bmatrix} i_{s\alpha}(k+1) \\ i_{s\beta}(k+1) \end{bmatrix} = (1 - \frac{RT_s}{L_s})\begin{bmatrix} 1 & 0 \\ 0 & 1 \end{bmatrix}\begin{bmatrix} i_{s\alpha}(k) \\ i_{s\beta}(k) \end{bmatrix} + \frac{T_s}{L_s}\begin{bmatrix} 1 & 0 \\ 0 & 1 \end{bmatrix}\begin{bmatrix} u_{s\alpha}(k) \\ u_{s\beta}(k) \end{bmatrix} - \frac{T_s}{L_s}\begin{bmatrix} 1 & 0 \\ 0 & 1 \end{bmatrix}\begin{bmatrix} v_{s\alpha}(k) \\ v_{s\beta}(k) \end{bmatrix} \qquad (21)$$

where $i_{s\alpha\beta}$ are the inverter-side currents, $u_{s\alpha\beta}$ are the inverter PWM voltages, $v_{s\alpha\beta}$ are the filter capacitor voltages and L_s and R are the filter components.

For the Slave, the current references in $\alpha\beta$ coordinates are also calculated from the instantaneous PQ theory as:

$$i_{so\alpha}^*(k) = \frac{2}{3}\frac{v_{s\alpha}(k)P_s^*(k) + v_{s\beta}(k)Q_s^*(k)}{v_{s\alpha}^2(k) + v_{s\beta}^2(k)} \qquad (22)$$

$$i_{so\beta}^*(k) = \frac{2}{3}\frac{v_{s\beta}(k)P_s^*(k) - v_{s\alpha}(k)Q_s^*(k)}{v_{s\alpha}^2(k) + v_{s\beta}^2(k)} \qquad (23)$$

When in grid-connected mode, P_s^* and Q_s^* can come from an MGCC; when islanded, they are set as half the active and reactive load powers so that the inverters can perform power sharing. As for the Master, $i_{so\alpha}^*(k)$ and $i_{so\beta}^*(k)$ are the grid-side current references, but the inverter-side currents are controlled. The voltages of the LCL filter capacitors are considered disturbances. The inverter-side current references are obtained from (22)-(23) by compensating the reactive power of the LCL filter capacitors:

$$i_{s\alpha}^*(k) = i_{so\alpha}^*(k) - 2\pi f C_s v_{s\beta}(k) \qquad (24)$$

$$i_{s\beta}^*(k) = i_{so\beta}^*(k) + 2\pi f C_s v_{s\alpha}(k) \qquad (25)$$
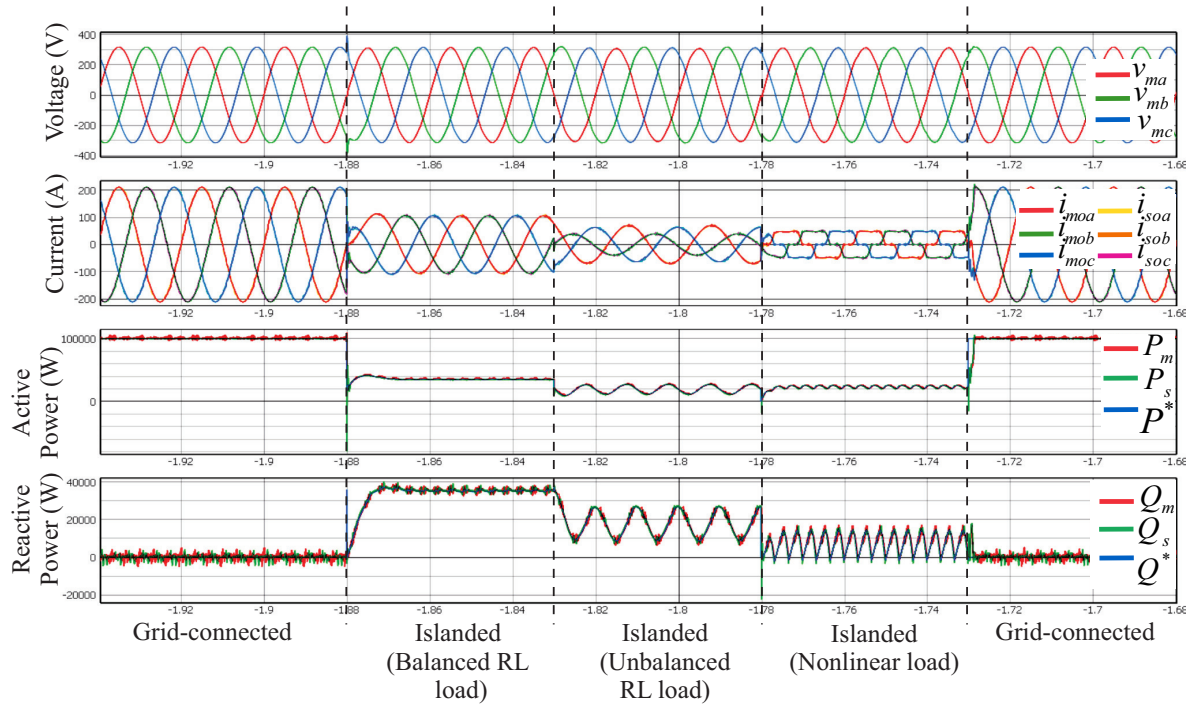
FIGURE 4. Results for the proposed Master-Slave FSF-MPC.
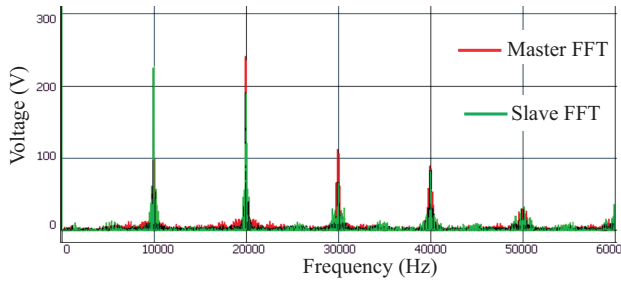
FIGURE 5. Zoom in the FFT of the output line-to-line voltages v_{ab} of the Master and Slave inverters for the proposed Master-Slave FSF-MPC.

where f is the grid frequency and C_s is the filter capacitance. Then, the references are extrapolated to (k+1):

$$i^*_{s\alpha}(k+1) = i^*_{s\alpha}(k)cos(\omega T_s) - i^*_{s\beta}(k)sin(\omega T_s) \qquad (26)$$

$$i^*_{s\beta}(k+1) = i^*_{s\beta}(k)cos(\omega T_s) + i^*_{s\alpha}(k)sin(\omega T_s) \qquad (27)$$

For the Slave, the cost function can be defined as the difference between the inverter-side current references $i^*_{s\alpha\beta}(k+1)$ and the predicted currents:

$$g_{sj} = (\mathbf{i}^*_{s\alpha\beta}(k+1) - \mathbf{i}_{sj\alpha\beta}(k+1))^2 + lim \qquad (28)$$

where $j = 0...7$ are the voltage vectors and $\mathbf{i}_{sj\alpha\beta}(k+1)$ are the predicted inverter-side currents for vector j. For each T_s, the inverter-side currents are predicted for all 8 inverter voltage vectors with (21), and the cost function (28) is calculated. The same switching sequences of Table 1 are used. Then, a sector and its respective switching sequence are selected. Again, the duty cycles are [16]:

$$d_a = \frac{g_{sb}g_{sc}}{G} \quad d_b = \frac{g_{sa}g_{sc}}{G} \quad d_c = \frac{g_{sa}g_{sb}}{G} \qquad (29)$$
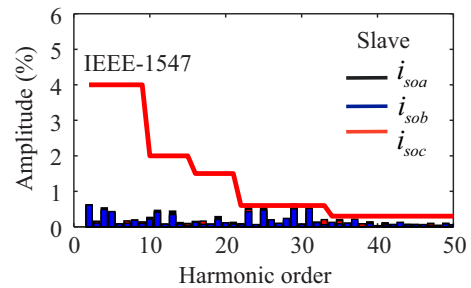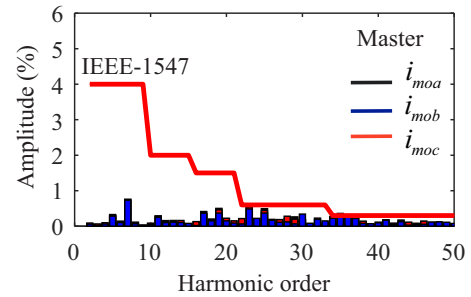
FIGURE 6. Individual current harmonic components and limits imposed by standard IEEE-1547 for grid-connected mode.

$$G = (g_{sb}g_{sc} + g_{sa}g_{sc} + g_{sa}g_{sb}) \qquad (30)$$

where $d_a + d_b + d_c = 1$. The cost function of each sector is:

$$g_{ss} = d_a g_{sa} + d_b g_{sb} + d_c g_{sc} \qquad (31)$$

where $s = 1...6$ are the sectors of the SV diagram and a, b, c represent the three vectors in each sector shown in Table 1. Finally, the sector with the lowest cost function is selected,
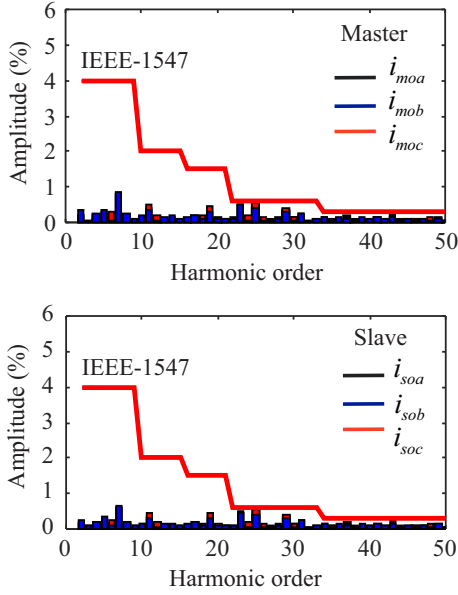
FIGURE 7. Individual current harmonic components and limits imposed by standard IEEE-1547 for islanded mode with balanced RL load.

and its switching sequence is implemented over the next T_s. This is depicted in the lower part of Fig.2.

III. CASE STUDIES

To demonstrate the performance of the proposed Master-Slave FSF-MPC, the microgrid of Fig.1 was implemented in a Typhoon HIL 604 Hardware-in-the-Loop (HIL). The system parameters are shown in Table 2. The control algorithms were implemented in the ARM processing core of Typhoon HIL, and the implementation delay of the processor was considered. Consequently, the cost functions are calculated for the predicted currents at $k+2$ and predicted voltages at $k+3$. The system disturbances are also estimated accordingly: the grid voltages for $k+3$, the Master grid-side currents for $k+2$, and the Slave capacitor voltages for $k + 2$. The weighting factors for cost function (11) were heuristically defined. For grid-connected mode, we have $\lambda_1 = 400$ and $\lambda_2 = 800$, and, for islanded mode, $\lambda_1 = 1000$ and $\lambda_2 = 400$.

Initially, the microgrid is connected to the grid. The Master and Slave are grid-following inverters, injecting 100kW and 0Var into the grid. The results are presented in Fig.4, which shows the Master capacitor voltages, the Master and Slave grid-side currents, and the active and reactive powers and their references (equal for both inverters). Then, the microgrid is islanded. The Master now is a grid-forming inverter, providing the microgrid voltages and half the total load power. The Slave is a grid-following inverter that also provides half the total load power. A balanced RL load ($R_l = 1.03\Omega$ and $L_l = 3.33$mH) is connected to the microgrid. Then, it changes to an unbalanced RL load ($R_l = 1.03\Omega$ and $L_l = 3.33$mH for phase a, $R_l = 4\Omega$ and $L_l = 10$mH for phase b and $R_l = 1.5\Omega$ and $L_l = 5$mH for phase c), and to a non-linear load comprised of a three-

phase diode rectifier with input L filter of 1mH and an RL load ($R = 5\Omega$, and $L = 5$mH). Finally, the microgrid is reconnected to the grid.

In Fig.4, the fast transition from grid-connected to islanded mode is seen. Similar behavior happens in islanded mode during load variations and when the microgrid is reconnected to the grid. The response times were measured from the instant when the change is applied to the time when the active and reactive powers reach the new steady-state: i) Grid-connected to islanded: 17.9ms; ii) First load change: 2.92ms; iii) Second load change: 5.37ms, iv) Islanded to grid-connected: 2.10ms. The output active and reactive powers of both inverters follow the references for both modes and all load conditions. In islanded mode, the Master can provide proper voltages to the microgrid. In addition, in the formulation of the FSF-MPC shown in Section II, the load is an unknown parameter for both inverters. Consequently, Fig.4 shows the good performance of the proposed FSF-MPC for different load variations and unmodeled dynamics.

The fixed switching frequency is validated by the spectra of the inverter output line-to-line voltages, measured before the filters. Fig.5 shows the FFTs of the output line-to-line voltages v_{ab} of the Master and Slave. The first significant harmonics appear at 10kHz. The voltage THD is 73.21% for the Master and 88.93% for the Slave. The THDs of the voltages of the Master capacitors and the grid-side currents of both inverters are shown in Tables 4 and 5, for, respectively, grid-connected and islanded mode with balanced RL load. The individual current harmonics are plotted in Figs. 6 and 7, and compared to the limits of IEEE-1547 [27]. It is seen that the harmonics are within the limits imposed by IEEE-1547. For islanded mode, there are slightly more distortions in the Master currents, which can be seen in the harmonic components and the THDs; the Slave has similar THDs for both modes, and the THD of the Master voltages are slightly higher for islanded mode.

TABLE 3. THD of the grid-side currents and filter voltages for grid-connected mode and islanded mode with balanced RL load.

Grid-connected	Master voltage	Master current	Slave current
phase a	0.27%	1.62%	1.90%
phase b	0.27%	1.62%	1.72%
phase c	0.27%	1.51%	1.77%
Islanded	**Master voltage**	**Master current**	**Slave current**
phase a	1.00%	1.78%	1.65%
phase b	0.99%	1.84%	1.72%
phase c	0.95%	1.75%	1.62%

Then, the parameters of the filters were decreased 50%, resulting in values of the LC filter as $R = 0.006\Omega$, $L = 250\mu H$ and $C = 150\mu F$, and of the LCL filter are $R = 0.006\Omega$, $L_1 = 250\mu H$, $L_2 = 25\mu H$ and $C = 50\mu F$. The results are shown in Fig.9. As the filter parameters are lower, there is a larger ripple on the active and reactive powers and the grid-side currents, as well as larger steady-state tracking

6

Eletrônica de Potência, Rio de Janeiro, v. 29, e202430, 2024.
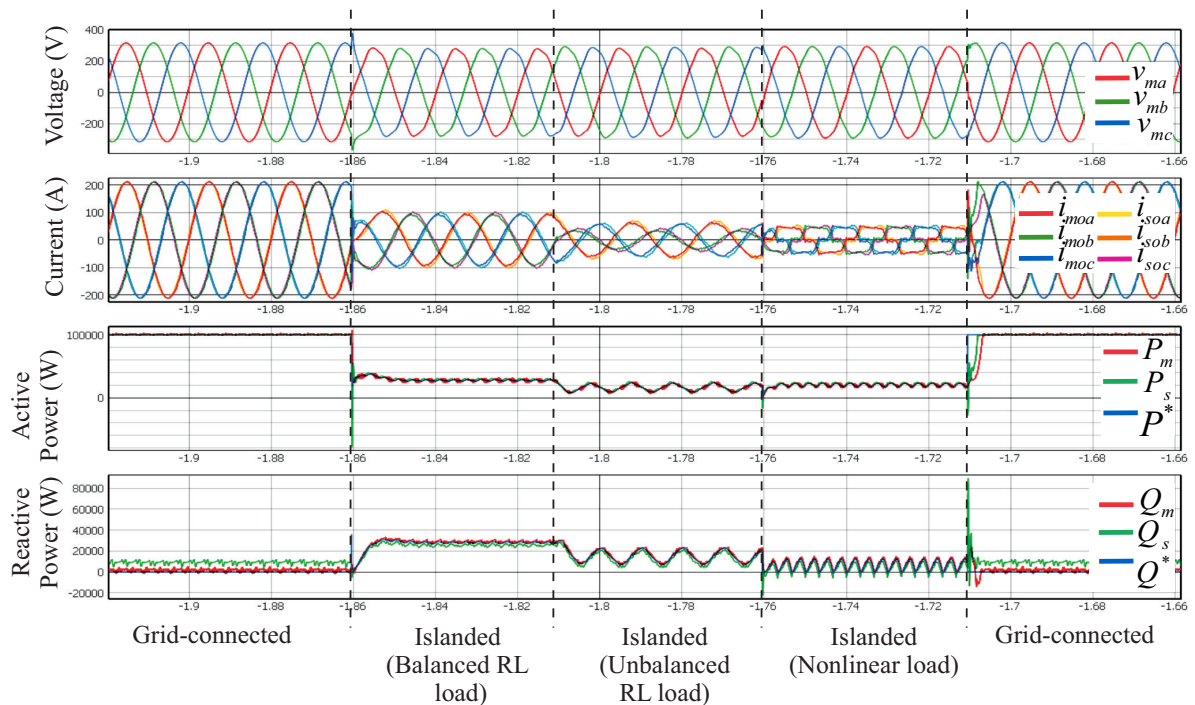
FIGURE 8. Results for the proposed Master-Slave FSF-MPC with higher filter parameters.
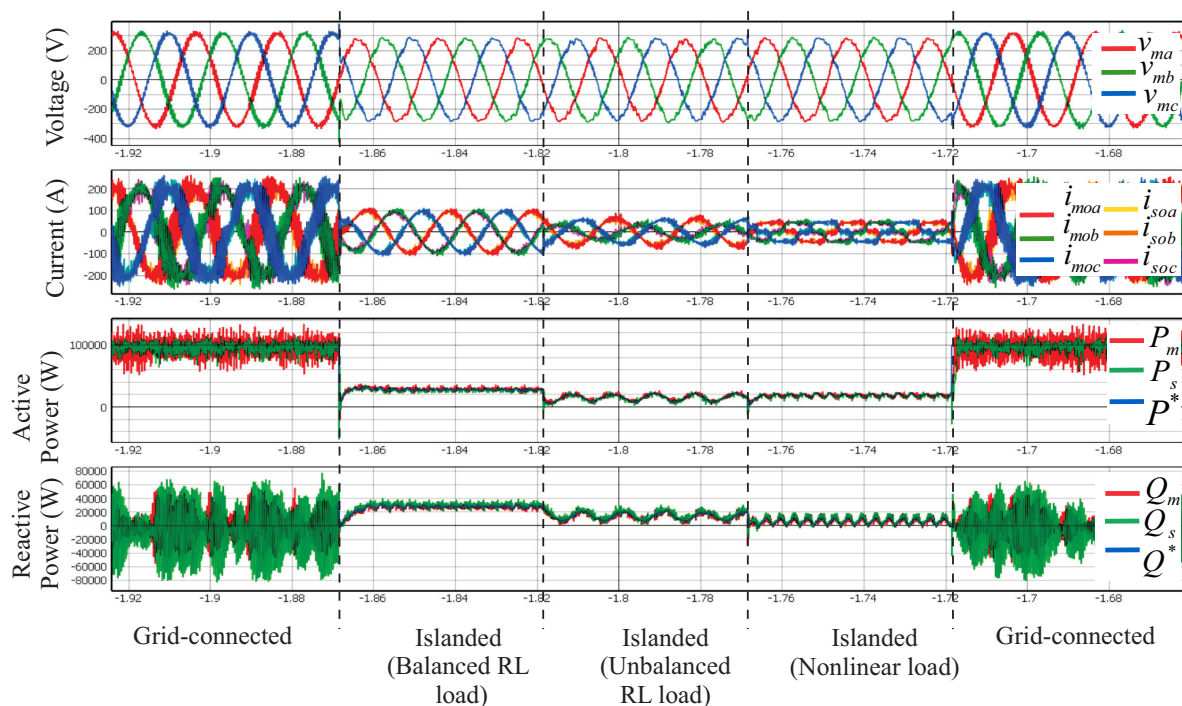
FIGURE 9. Results for the proposed Master-Slave FSF-MPC with lower filter parameters.

errors. This is more accentuated resonances of the filter and grid impedances. In islanded mode, there is again a drop in the voltages and more distortions when compared to nominal operation. These can now be attributed to the lower filter capacitance, which is not able to hold the microgrid voltage properly.

The higher steady-state tracking error for both parameter mismatches happens due to the variations in the filter capacitance, which is used to calculate the inverter-side current references. However, the system remains stable even with high parameter mismatches. It is difficult to prove the stability of systems with MPC in a closed form, and stability
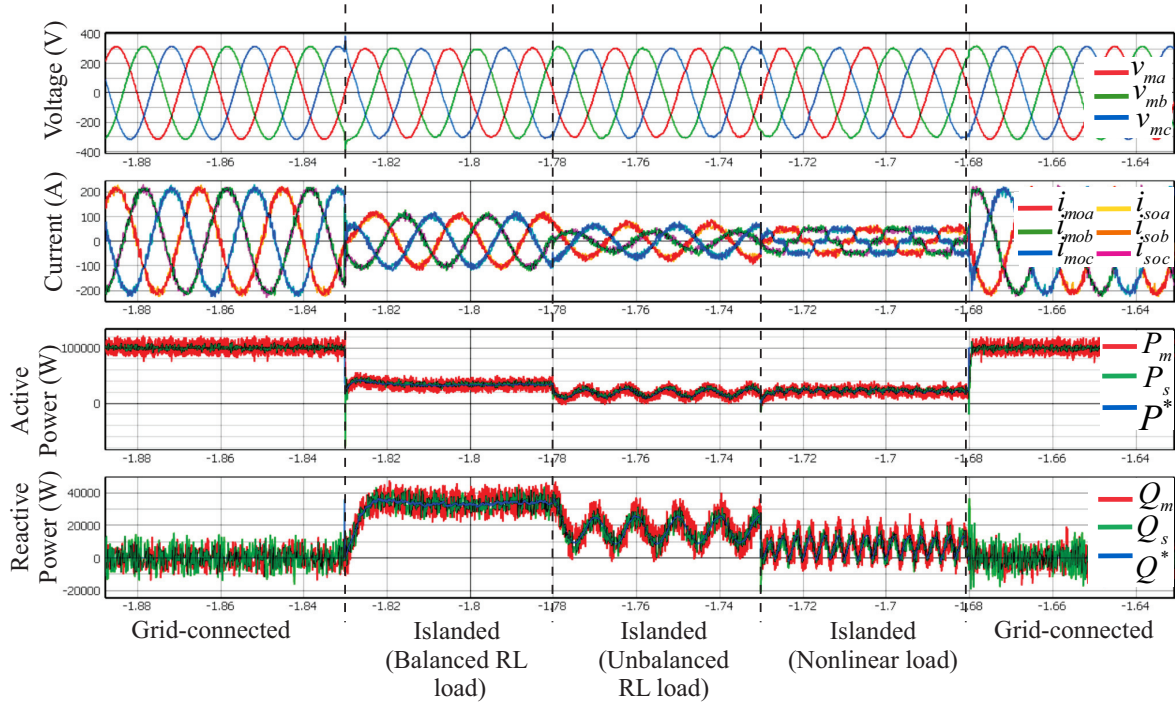
FIGURE 10. Results for the Master-Slave FCS-MPC of [28].

TABLE 4. THD of the grid-side currents and filter voltages for grid-connected mode.

	Master voltage	Master current	Slave current
phase a	0.27%	1.62%	1.90%
phase b	0.27%	1.62%	1.72%
phase c	0.27%	1.51%	1.77%

TABLE 5. THD of the grid-side currents and filter voltages for islanded mode with balanced RL load.

	Master voltage	Master current	Slave current
phase a	1.00%	1.78%	1.65%
phase b	0.99%	1.84%	1.72%
phase c	0.95%	1.75%	1.62%
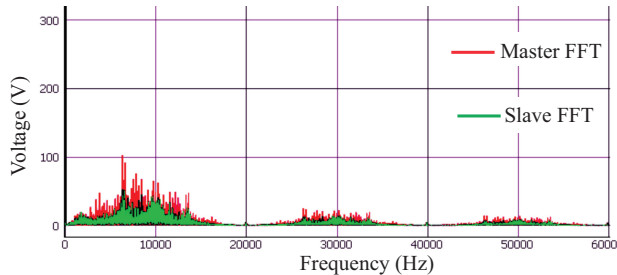
FIGURE 11. Zoom in the FFT of the output line-to-line voltages v_{ab} of the Master and Slave inverters for the Master-Slave FCS-MPC of [28].

assessment of MPC is still an open area of research. Usually, stability assessment of MPC is done empirically [29], [30], as it is done in this work. It can be stated that the proposed FSF-MPC is stable for the system considered in this analysis.

Let us now compare the Master-Slave FSF-MPC with the Master-Slave FCS-MPC of [28]. The same case studies were applied to the FCS-MPC, also considering the same parameters of Table 2. These results are shown in Fig.10. As the FCS-MPC implements only one voltage vector per T_s, the output currents of the Master and Slave have very large ripples, which also appear at the active and reactive powers. Also, the FCS-MPC results in variable switching frequency and widespread harmonic content. The variable switching frequency is seen in Fig.11, which shows the FFTs of the output line-to-line voltages v_{ab} of the Master and Slave. For the Master, the equivalent switching frequency is around 8kHz, while for the Slave, it is around 10kHz. The voltage THDs are 91.07% for the Master and 102.79% for the Slave. The average THD of the output currents is 7.99% for the Master and 8.41% for the Slave. It can be observed that the FCS-MPC has higher values of THD for voltages and currents for the same system parameters. Consequently, the results presented in this paper demonstrate the good performance of the proposed Master-Slave FSF-MPC for microgrids.

IV. CONCLUSIONS

This paper proposed a Fixed-Switching-Frequency Model Predictive Control (FSF-MPC) for Master-Slave inverters in microgrids. To validate the proposed FSF-MPC, Hardware-in-the-Loop results using a Typhoon HIL 604 were presented for different operational conditions, including grid-connected and islanded modes. The results presented demonstrate the good performance of the proposed Master-Slave FSF-MPC,

8

Eletrônica de Potência, Rio de Janeiro, v. 29, e202430, 2024.

including fast dynamic response, robustness against load variations, parameter mismatches and unmodeled dynamics, and fixed switching frequency.

V. AKNOWLEDGEMENTS

AUTHOR CONTRIBUTIONS

CARNIELUTTI, F.: Conceptualization, Data Curation, Formal Analysis, Funding Acquisition, Investigation, Methodology, Project Administration, Resources, Software, Supervision, Validation, Visualization, Writing – Original Draft, Writing – Review & Editing. **ALY, M.**: Conceptualization, Formal Analysis, Investigation, Methodology, Software, Validation, Visualization, Writing – Review & Editing. **NORAMBUENA, M.**: Conceptualization, Formal Analysis, Investigation, Methodology, Software, Validation, Visualization, Writing – Review & Editing. **HU, J.**: Conceptualization, Formal Analysis, Investigation, Methodology, Writing – Review & Editing. **GUERRERO, J.**: Conceptualization, Formal Analysis, Investigation, Methodology, Writing – Review & Editing. **RODRIGUEZ, J.**: Conceptualization, Formal Analysis, Funding Acquisition, Investigation, Methodology, Project Administration, Supervision, Writing – Review Editing.

PLAGIARISM POLICY

REFERENCES

[1] Z. Zhang, O. Babayomi, T. Dragicevic, R. Heydari, C. Garcia, J. Rodriguez, R. Kennel, "Advances and opportunities in the model predictive control of microgrids: Part I–primary layer", *International Journal of Electrical Power Energy Systems*, vol. 134, p. 107411, 2022.

[2] J. G. J. Hu, S. Islam, *Model Predictive Control For Microgrids - From Power Electronics Converters to Energy Management*, IET - The Institution of Engineering and Technology, 2021.

[3] P. Buduma, M. K. Das, R. T. Naayagi, S. Mishra, G. Panda, "Seamless Operation of Master–Slave Organized AC Microgrid With Robust Control, Islanding Detection, and Grid Synchronization", *IEEE Transactions on Industry Applications*, vol. 58, no. 5, pp. 6724–6738, Sep. 2022, doi:10.1109/tia.2022.3185575.

[4] A. Mortezaei, M. G. Simoes, M. Savaghebi, J. M. Guerrero, A. Al-Durra, "Cooperative Control of Multi-Master–Slave Islanded Microgrid With Power Quality Enhancement Based on Conservative Power Theory", *IEEE Transactions on Smart Grid*, vol. 9, no. 4, pp. 2964–2975, Jul. 2018, doi:10.1109/tsg.2016.2623673.

[5] D. Miller, G. Mirzaeva, C. D. Townsend, G. C. Goodwin, "Decentralised Droopless Control of Islanded Radial AC Microgrids Without Explicit Communication", *IEEE Open Journal of Industry Applications*, vol. 3, pp. 104–113, 2022, doi:10.1109/ojia.2022.3177857.

[6] Y. Yang, R.-J. Wai, "Self-Constructing Fuzzy-Neural-Network-Imitating Sliding-Mode Control for Parallel-Inverter System in Grid-Connected Microgrid", *IEEE Access*, vol. 9, pp. 167389–167411, 2021, doi:10.1109/access.2021.3135856.

[7] D.-D. Zheng, S. S. Madani, A. Karimi, "Data-Driven Distributed Online Learning Control for Islanded Microgrids", *IEEE Journal on Emerging and Selected Topics in Circuits and Systems*, vol. 12, no. 1, pp. 194–204, Mar. 2022, doi:10.1109/jetcas.2022.3152938.

[8] J. Rodriguez, M. P. Kazmierkowski, J. R. Espinoza, P. Zanchetta, H. Abu-Rub, H. A. Young, C. A. Rojas, "State of the Art of Finite Control Set Model Predictive Control in Power Electronics", *IEEE Trans Ind Informat*, vol. 9, no. 2, pp. 1003–1016, May. 2013.

[9] P. Karamanakos, E. Liegmann, T. Geyer, R. Kennel, "Model Predictive Control of Power Electronic Systems: Methods, Results, and Challenges", *IEEE Open J Ind Appl*, vol. 1, pp. 95–114, Aug. 2020, doi:10.1109/OJIA.2020.3020184.

[10] J. Scoltock, T. Geyer, U. K. Madawala, "Model Predictive Direct Power Control for Grid-Connected NPC Converters", *IEEE Transactions on Industrial Electronics*, vol. 62, no. 9, pp. 5319–5328, 2015, doi:10.1109/TIE.2015.2410259.

[11] Y. Shan, J. Hu, Z. Li, J. M. Guerrero, "A Model Predictive Control for Renewable Energy Based AC Microgrids Without Any PID Regulators", *IEEE Transactions on Power Electronics*, vol. 33, no. 11, pp. 9122–9126, 2018, doi:10.1109/TPEL.2018.2822314.

[12] T. Dragičević, "Model Predictive Control of Power Converters for Robust and Fast Operation of AC Microgrids", *IEEE Transactions on Power Electronics*, vol. 33, no. 7, pp. 6304–6317, 2018, doi:10.1109/TPEL.2017.2744986.

[13] A. Venkat, I. Hiskens, J. Rawlings, S. Wright, "Distributed MPC Strategies With Application to Power System Automatic Generation Control", *IEEE Transactions on Control Systems Technology*, vol. 16, no. 6, pp. 1192–1206, Nov. 2008, doi:10.1109/tcst.2008.919414.

[14] Y. Shan, J. Hu, H. Liu, "A Holistic Power Management Strategy of Microgrids Based on Model Predictive Control and Particle Swarm Optimization", *IEEE Transactions on Industrial Informatics*, vol. 18, no. 8, pp. 5115–5126, 2022, doi:10.1109/TII.2021.3123532.

[15] J. Sachs, O. Sawodny, "A Two-Stage Model Predictive Control Strategy for Economic Diesel-PV-Battery Island Microgrid Operation in Rural Areas", *IEEE Transactions on Sustainable Energy*, vol. 7, no. 3, pp. 903–913, 2016, doi:10.1109/TSTE.2015.2509031.

[16] Y. Yang, J. Pan, H. Wen, X. Zhang, M. Norambuena, L. Xu, J. Rodriguez, "Computationally Efficient Model Predictive Control With Fixed Switching Frequency of Five-Level ANPC Converters", *IEEE Trans on Ind Electronics*, vol. 69, no. 12, pp. 11903–11914, 2022, doi:10.1109/TIE.2021.3131797.

[17] D. Schuetz, C. R. D. Osório, L. A. Maccari, D. M. Lima, F. d. M. Carnielutti, V. F. Montagner, H. Pinheiro, "Space Vector Modulated Model Predictive Control for Grid-Tied Converters", *IEEE Transactions on Industrial Informatics*, vol. 19, no. 1, pp. 414–425, 2023, doi:10.1109/TII.2022.3193674.

[18] J. Xu, T. B. Soeiro, F. Gao, L. Chen, H. Tang, P. Bauer, T. Dragicevic, "Carrier-Based Modulated Model Predictive Control Strategy for Three-Phase Two-Level VSIs", *IEEE Transactions on Energy Conversion*, vol. 36, no. 3, pp. 1673–1687, Sep. 2021, doi:10.1109/tec.2021.3073110.

[19] C. F. Garcia, C. A. Silva, J. R. Rodriguez, P. Zanchetta, S. A. Odhano, "Modulated Model-Predictive Control With Optimized Overmodulation", *IEEE Journal of Emerging and Selected Topics in Power Electronics*, vol. 7, no. 1, pp. 404–413, Mar. 2019, doi:10.1109/jestpe.2018.2828198.

[20] N. Jin, M. Chen, L. Guo, Y. Li, Y. Chen, "Double-Vector Model-Free Predictive Control Method for Voltage Source Inverter With Visualization Analysis", *IEEE Transactions on Industrial Electronics*, vol. 69, no. 10, pp. 10066–10078, Oct. 2022, doi:10.1109/tie.2021.3128905.

[21] M. Aly, F. Carnielutti, A. Shawky, E. M. Ahmed, M. Norambuena, S. Kouro, J. Rodriguez, "Weighting Factorless Sequential Model Predictive Control Method with Fixed Switching Frequency for Five-Level T-type Photovoltaic Inverters", *in IECON 2021 – 47th Annual Conference of the IEEE Industrial Electronics Society*, pp. 1–6, 2021, doi:10.1109/IECON48115.2021.9589758.

[22] M. Aly, F. Carnielutti, M. Norambuena, E. M. Ahmed, S. Kouro, J. Rodriguez, "Fixed Switching Frequency Model Predictive Controller for Doubly-Grounded Five-Level Photovoltaic Inverter", *in 2021 IEEE 12th Energy Conversion Congress Exposition - Asia (ECCE-Asia)*, pp. 932–937, 2021, doi:10.1109/ECCE-Asia49820.2021.9479061.

[23] F. Carnielutti, M. Aly, M. Norambuena, J. Hu, J. Guerrero, J. Rodriguez, "Model Predictive Control of Master-Slave Inverters Operating with Fixed Switching Frequency", *in 2023 IEEE*

8th Southern Power Electronics Conference and 17th Brazilian Power Electronics Conference (SPEC/COBEP), pp. 1–6, 2023, doi:10.1109/SPEC56436.2023.10408203.

[24] R. Teodorescu, M. Liserre, P. Rodriguez, *Grid Converters for Photovoltaic and Wind Power Systems*, Wiley-IEEE Press, 2007.

[25] T. Dragičević, "Model Predictive Control of Power Converters for Robust and Fast Operation of AC Microgrids", *IEEE Transactions on Power Electronics*, vol. 33, no. 7, pp. 6304–6317, 2018, doi:10.1109/TPEL.2017.2744986.

[26] R. Heydari, T. Dragicevic, F. Blaabjerg, "High-Bandwidth Secondary Voltage and Frequency Control of VSC-Based AC Microgrid", *IEEE Transactions on Power Electronics*, vol. 34, no. 11, pp. 11320–11331, 2019, doi:10.1109/TPEL.2019.2896955.

[27] "IEEE Standard for Interconnection and Interoperability of Distributed Energy Resources with Associated Electric Power Systems Interfaces", *IEEE Std 1547-2018 (Revision of IEEE Std 1547-2003)*, pp. 1–138, 2018, doi:10.1109/IEEESTD.2018.8332112.

[28] F. Carnielutti, M. Aly, M. Norambuena, J. Rodriguez, "Model Predictive Control for Master-Slave Inverters in Microgrids", *in IECON 2022 – 48th Annual Conference of the IEEE Industrial Electronics Society*, pp. 1–6, 2022, doi:10.1109/IECON49645.2022.9968694.

[29] S. Vazquez, J. Rodriguez, M. Rivera, L. G. Franquelo, M. Norambuena, "Model Predictive Control for Power Converters and Drives: Advances and Trends", *IEEE Trans Ind Electron*, vol. 64, no. 2, pp. 935–947, Feb. 2017, doi:10.1109/TIE.2016.2625238.

[30] R. E. Pérez-Guzmán, M. Rivera, P. W. Wheeler, "Recent Advances of Predictive Control in Power Converters", *in 2020 IEEE International Conference on Industrial Technology (ICIT)*, pp. 1100–1105, 2020, doi:10.1109/ICIT45562.2020.9067169.

BIOGRAPHIES

Fernanda Carnielutti received the bachelor degree in electrical engineering in 2010 from the Federal University of Santa Maria (UFSM), Santa Maria, Brazil, where she received the master and doctoral degrees in electrical engineering in 2012 and 2015. She is currently a Professor with the Federal University of Santa Maria and a Researcher with the Power Electronics and Control Research Group (GEPOC), UFSM. Her research interests include modulation of static power converters, multilevel converters power electronics for renewable energies, microgrids and model predictive control. Dr. Carnielutti is a member of the IEEE Power Electronics Society, the IEEE Industrial Electronics Society, the IEEE Industry Applications Society, and the Associação Brasileira de Eletrônica de Potência.

Mokhtar Aly received the B.Sc. and M.Sc. degrees in electrical engineering from Aswan University, Aswan, Egypt, in 2007 and 2012 and the Ph.D. degree from the Department of Electrical Engineering, Faculty of Information Science and Electrical Engineering, Kyushu University, Japan in 2017. In 2008, he joined the Department of Electrical Engineering, Aswan University, as an Assistant Lecturer, where he has been an Assistant Professor with the Faculty of Engineering since 2017. He worked as a Postdoctoral Researcher with the Solar Energy Research Center (SERC-Chile), Universidad Técnica Federico Santa María, Chile from 2019 to 2021. He is currently an Assistant Professor with Universidad San Sebastián, Santiago, Chile since 2021. His research interests include reliability of power electronics systems in renewable energy applications, multi-level inverters, fault tolerant control, electric vehicles and light emitting diode (LED) drivers. He is a member in IEEE Power Electronics Society (PELS), IEEE Industrial Electronics Society (IES), and IEEE Power and Energy Society (PES).

Margarita Norambuena Margarita Norambuena received the B.S. and M. Sc. degrees in electrical engineering from the Universidad Tecnica Federico Santa Maria (UTFSM), Valparaiso, Chile, in 2013. She received her Ph.D. degree (summa cum laude) in electronics engineering from the UTFSM in 2017. She received the Doktoringenieur (Dr-Ing.) degree (summa cum laude) from the Technische Universitat Berlin (TUB) in 2018. She received the IEEE IES Student Best Paper Award 2019 for her doctoral work. She is an Assistant Professor at Universidad Tecnica Federico Santa Maria. Her research interest are multilevel converters, model predictive control of power converters and drives, energy storage systems, renewable energy, and electromobility. Dr. Norambuena is Associate Editor for IEEE JESTPE.

Jiefeng Hu received a Ph.D. degree in electrical engineering from University of Technology Sydney, Australia. He participated in minigrids research at Commonwealth Scientific and Industrial Research Organization, Newcastle, Australia. He was Assistant Professor at The Hong Kong Polytechnic University, Kowloon, Hong Kong. He is currently Associate Professor and Program Coordinator of Electrical Engineering at Federation University Australia, Ballarat, VIC, Australia, where he is also a Stream Leader of Centre for New Energy Transition Research. His research interests include power electronics, renewable energy, and smart microgrids. Dr. Hu is Associate Editor for IET Renewable Power Generation, Editor for IEEE Transactions on Energy Conversion, Associate Editor for IEEE Access, and was Guest Editor for IEEE Transactions on Industrial Electronics for a Special Issue "Applications of Predictive Control in Microgrids."

Josep Guerrero received the B.S. degree in telecommunications engineering, the M.S. degree in electronics engineering, and the Ph.D. degree in power electronics from the Technical University of Catalonia, Barcelona, in 1997, 2000, and 2003. Since 2011, he is Full Professor at the Department of Energy Technology, Aalborg University, Denmark, where he is responsible for the Microgrid Research Program. He is Chair Professor with Shandong University since 2014, Distinguished Guest Professor with Hunan University since 2015, Visiting Professor Fellow with Aston University, U.K., since 2016, and Guest Professor with the Nanjing University of Posts and Telecommunications. In 2019, he became a Villum Investigator. He has published more than 500 journal articles in the fields of microgrids and renewable energy systems. His research interests are different microgrid aspects, including power electronics, distributed energy storage systems, hierarchical and cooperative control, energy management systems, smart metering, Internet of Things for AC/DC microgrid clusters and islanded minigrids, recently focusing on maritime microgrids for electrical ships, vessels, ferries, and seaports. In 2015, he was elevated to IEEE Fellow for his contributions on "Distributed power systems and microgrids." He received the Best Paper Award of IEEE Transactions on Energy Conversion from 2014 to 2015, the Best Paper Prize of IEEE-PES in 2015, and the Best Paper Award of the Journal of Power Electronics in 2016. For five consecutive years, from 2014 to 2018, he was awarded by Clarivate Analytics (former Thomson Reuters) as the Highly Cited Researcher. He is an associate editor for a number of IEEE Transactions.

José Rodriguez received the Engineer degree in electrical engineering from the Universidad Tecnica Federico Santa Maria, in Valparaiso, Chile, in 1977 and the Dr.-Ing. degree in electrical engineering from the University of Erlangen, Erlangen, Germany, in 1985. He has been with the Department of Electronics Engineering, Universidad Tecnica Federico Santa Maria, since 1977, where he was full Professor and President. From 2015 to 2019, he was the President of Universidad Andres Bello in Santiago, Chile. From 2022 to 2023, he was President of Universidad San Sebastian in Santiago, Chile. Now, he is the Director of the Center for Energy Transition at Universidad San Sebastian. He has coauthored two books, several book chapters and

more than 900 journal and conference papers. His main research interests include multilevel inverters, new converter topologies, control of power converters and adjustable-speed drives. He has received a number of best paper awards from IEEE journals. Dr. Rodriguez is member of the Chilean Academy of Engineering. In 2014 he received the National Award of Applied Sciences and Technology from the government of Chile. In 2015 he received the Eugene Mittelmann Award from the Industrial Electronics Society of the IEEE. In years 2014 to 2023, he was included in the list of Highly Cited Researchers published by Web of Science.